Superconductivity coupled to density waves

Nobuhiro Mitani and Susumu Kurihara
NTT Basic Research Laboratories, Musashino, Tokyo 180, Japan
(Received 3 March 1993)

We investigate a mechanism of superconductivity on the basis of the nested-Fermi-liquid theory. A set of parquet equations is derived to investigate the instability towards superconductivity and spin- or charge-density-wave states. The phase diagram is examined on the basis of the parquet equations. We find that the polarization mode of the marginal-Fermi-liquid-type is of vital importance to superconductivity. We also discuss the properties of a superconductor on the basis of the nested Fermi liquid.

I. INTRODUCTION

Varma *et al.*[1] proposed a phenomenological theory describing a type of liquid state called marginal Fermi liquid (MFL) to account for anomalous properties in the normal state of oxide superconductors. They introduced a polarization propagator P which has an unusual dependence on frequency:

$$\mathrm{Im}P_R(\omega,\mathbf{q}) \sim \begin{cases} -N(0)\frac{\omega}{k_BT} & \text{for } |\omega| \le k_BT, \\ -N(0)\mathrm{sgn}\omega & \text{for } |\omega| \ge k_BT, \end{cases} \quad (1)$$

where $N(0)$ is the density of states at the Fermi level. In a one-loop approximation, this causes a logarithmic singularity in electron self-energy at low energies, and the quasiparticle picture breaks down; the liquid is no longer a Fermi liquid. The MFL theory has been successful in explaining anomalous normal-state properties.

The scaling properties of the MFL have been investigated by Zimanyi and Bedell[2] by the renormalization group method. On the other hand, we have shown[3] that the vertex renormalization is very important; it causes a crossover in low-energy behavior from the MFL to the usual Fermi liquid with a finite effective mass and a quasiparticle residue. This comes essentially from screening effects by particle hole pairs near the Fermi surface.

Virosztek and Ruvalds[4] have proposed a microscopic mechanism leading to the MFL anomaly; near half filling, nesting of the Fermi surface could cause a polarization mode of the MFL type. The microscopic mechanism is called the nested-Fermi-liquid (NFL) theory. We expect a deep relation between the nested Fermi liquid and high-temperature superconductivity because of MFL-like behaviors of normal states.

In the present paper, we investigate the superconducting instability on the basis of the NFL theory in more detail. We study a few types of extended Hubbard models with a nearly half-filled band.

At half filling, the spin-density wave or charge-density wave [here after referred to as density wave (DW) for brevity] channel and superconducting channel are strongly coupled with each other, as shown in Fig. 2, leading to the parquet-type simultaneous divergences in both channels. Because of this, the hole liquid becomes a Luttinger liquid characterized by power-law divergence of various correlation functions, as was shown by Bychkov *et al.*[5–7] For finite doping, the Fermi surface is warped as shown in Fig. 1. Fermi surface nesting is then suppressed, and the DW singularity is cut off. We see that the normal state recovers the Fermi-liquid nature for sufficient doping.[3] For energies lower than a characteristic warping energy to be discussed shortly, NFL features are cut off. We will study the crossover from MFL at high energies to Fermi liquid at low energies.

We apply the parquet technique to the two-dimensional Hubbard model.[8,9] We find from our calculation that the Hubbard model has only magnetic orders such as SDW, and does not have a superconducting ground state.[10] Since we are interested in the superconducting phase, we shall add various terms (charge or spin fluctuation terms) which cause superconductivity to the Hubbard model. As an example of such models we first examine the Emery model[11–13] also by the parquet method. We show that the nearest-neighbor Coulomb term enhances the MFL-type polarization mode and at-

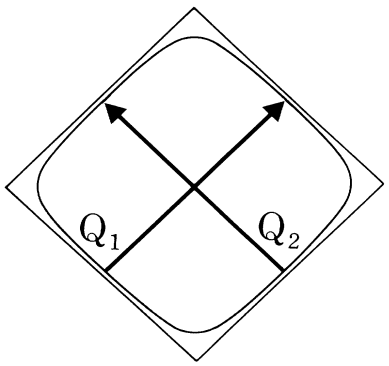

FIG. 1. Fermi surfaces represented in the magnetic Brillouin zone, and have two nesting vectors Q_1 and Q_2. The nested Fermi surface is warped by hole doping.

tractive forces between holes, thus favoring the high-T_C superconductivity. Next, we investigate the effects of spin fluctuation by using an extended Hubbard model with an Ising-type interaction. An antiferromagnetic (AFM) Ising interaction is found to enhance SDW and spin-singlet d-wave-like superconductivity (SC). The Fermi surface's warping effect screens the SDW singularity, but enhances spin-singlet d-wave-like SC. The ferromagnetic (FM) Ising interaction enhances spin-triplet p-wave-like SC and SDW.

In Sec. II, we calculate the parquet equations for the Hubbard model in order to study the interplay between superconductivity and SDW. In Sec. III, we investigate the Emery model by using the same method as in Sec. II. In Sec. IV, we also investigate the extended Hubbard model with an Ising-type interaction. In Sec. V, we discuss various properties of a superconductor coupled to the NFL. In Sec. VI, we summarize our results.

II. THE HUBBARD MODEL

In this section we investigate the Hubbard model[8,9] adopting the parquet method. Near half filling, two distinct kinds of instabilities, superconducting instability and density-wave instabilities (either SDW or CDW), occur simultaneously in particle-particle and particle-hole channels: both channels have logarithmic divergence near a half-filled band. It should be noted that, while Cooper instability is rather insensitive to the shape of the Fermi surface, the density-wave instability is quite easily suppressed by a small amount of doping because of the Fermi surface warping effect (see Fig. 1).

The complete nesting for an undoped system is cut off by a finite curvature of the Fermi surface when holes are doped. The logarithmic divergence at low energies (or at low temperatures) is cut off at a characteristic energy ω_0. In the logarithmic accuracy used in parquet equations, we are justified to identify ω_0 with the Fermi energy of holes, neglecting numerical factors of order unity:

$$\omega_0 \sim t\delta, \tag{2}$$

where t and δ are a hopping integral of holes and a amount of doped holes.

TABLE I. Definitions of two-body vertices. I and R stand for the irreducible and reducible vertices for each channel.

Mode \ Notation	γ^{I}	γ^{BCS}	γ^{DW}	Σ	S	γ
BCS	I	R	I	I	R or I	Total vertex
SDW or CDW	I	I	R	R or I	I	Total vertex

For later convenience we first give a very brief summary of parquet theory.[5,6] Let us assume that the momentum dependence of polarizability in the NFL is weak around two nesting vectors Q_1 and Q_2. We can classify all the interaction vertices logically either to reducible or irreducible sets by cutting two fermion line diagrams in DW or BCS channels. The classification is shown in Table I.

The total vertex part γ consists of three parts. The first is the sum of totally irreducible diagrams, which we denote by γ^{I}. The second is the sum of all vertices which are reducible in the DW channel, which is denoted by γ^{DW}. The third is the sum of all vertices which are reducible in the BCS channel, which is denoted by γ^{BCS} (Fig. 2):

$$\gamma = \gamma^{\mathrm{I}} + \gamma^{\mathrm{DW}} + \gamma^{\mathrm{BCS}}. \tag{3}$$

It follows that

$$\gamma = \Sigma + \gamma^{\mathrm{BCS}} = S + \gamma^{\mathrm{DW}}, \tag{4}$$

$$S = \gamma^{\mathrm{I}} + \gamma^{\mathrm{BCS}}, \tag{5}$$

$$\Sigma = \gamma^{\mathrm{I}} + \gamma^{\mathrm{DW}}, \tag{6}$$

where S and Σ are irreducible parts of the DW and BCS channels.

We can express these logical relations between vertices by a set of parquet equations, as shown diagrammatically in Fig. 3. The corresponding analytic expressions are given by

$$\bar{\gamma}^{\mathrm{DW}}_{\alpha\gamma\beta\delta}(\eta,\xi) = -\frac{i}{2\pi}\int d\omega\, d\varepsilon_{\mathbf{k}} G(\omega,\varepsilon_{\mathbf{k}}) G(\omega-\omega_1,\varepsilon_{\mathbf{k}-\mathbf{q}}) \bar{S}_{\alpha\gamma\theta\epsilon}(\eta,t)\bar{\gamma}_{\epsilon\theta\beta\delta}(\eta,t), \tag{7}$$

$$\gamma^{\mathrm{BCS}}_{\alpha\gamma\beta\delta}(\eta,\xi) = +\frac{i}{2\pi}\int d\omega\, d\varepsilon_{\mathbf{k}} G(\omega,\varepsilon_{\mathbf{k}}) G(\omega_2-\omega,\varepsilon_{\mathbf{k}-\mathbf{q}}) \Sigma_{\alpha\gamma\theta\epsilon}(t,\xi)\gamma_{\epsilon\theta\beta\delta}(t,\xi), \tag{8}$$

where quantities with or without the upper bar represent vertices in electron-hole or electron-electron channels, respectively. $t \equiv \ln\Lambda/\omega$. Energy variables, ω_1 and ω_2, are energies of the center of mass of the DW channel and the BCS channel, and are represented by corresponding logarithmic variables $\eta \equiv \ln\Lambda/\omega_1$ and $\xi \equiv \ln\Lambda/\omega_2$. We also define a logarithmic cutoff energy $\eta_0 \equiv \ln\Lambda/\omega_0$.

The vertices have the following "crossing" symmetry:

$$\bar{\gamma}_{\alpha\gamma\beta\delta}(\eta,\xi) = -\gamma_{\delta\gamma\beta\alpha}(\eta,\xi). \tag{9}$$

By using the symmetry, we can rewrite the parquet equations only in terms of vertices in the particle-particle channel (Fig. 3).

In order to study the effects of spin degrees of freedom, we decompose the vertices as follows:

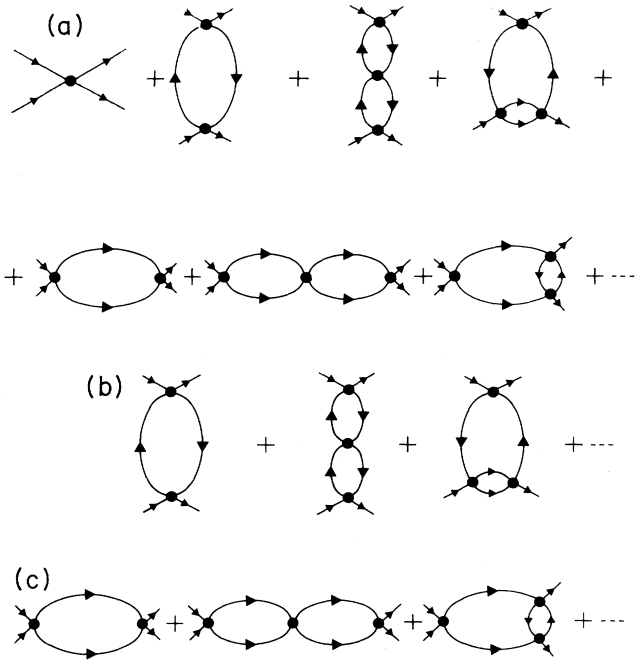

FIG. 2. Diagrammatic expansion of the vertex, (a) total vertex $\gamma(=R+\gamma^{\mathrm{DW}}+\gamma^{\mathrm{SC}})$, (b) reducible vertex for the DW channel γ^{DW}, (c) reducible vertex for the SC channel γ^{SC}.

$$\gamma_{\alpha\gamma\beta\delta}=\gamma_1(\delta_{\alpha\beta}\delta_{\gamma\delta}-\delta_{\alpha\delta}\delta_{\beta\gamma})+\gamma_2\delta_{\alpha\delta}\delta_{\gamma\beta}, \tag{10}$$

$$S_{\alpha\gamma\beta\delta}=s_1(\delta_{\alpha\beta}\delta_{\gamma\delta}-\delta_{\alpha\delta}\delta_{\beta\gamma})+s_2\delta_{\alpha\delta}\delta_{\gamma\beta}, \tag{11}$$

$$\Sigma_{\alpha\gamma\beta\delta}=\sigma_1(\delta_{\alpha\beta}\delta_{\gamma\delta}-\delta_{\alpha\delta}\delta_{\beta\gamma})+\sigma_2\delta_{\alpha\delta}\delta_{\gamma\beta}. \tag{12}$$

We have chosen tensor components in accordance with Bychkov *et al.* The components γ_1 and $\gamma_2-\gamma_1$ correspond to backward scattering g_1 and forward scattering g_2 as shown in Fig. 4.

A wide class of models, including the Hubbard model, can be properly treated by this decomposition, as long as they have rotational symmetry in spin space. An exceptional case will be discussed in Sec. IV.

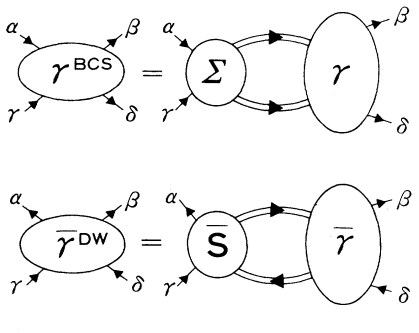

FIG. 3. Parquet diagrams.

In the parquet calculation with logarithmic accuracy we can make the following substitutions.[5,6]

In the case $\eta<\xi$,

$$\gamma^{\mathrm{DW}}(t,\xi)\rightarrow\gamma^{\mathrm{DW}}[\min(t,\eta),\xi], \tag{13}$$

$$\Sigma(t,\xi)\rightarrow\Sigma[\min(t,\eta),\xi]. \tag{14}$$

The BCS channel is crucial in this case, because the characteristic logarithmic energy becomes ξ. The case of $\xi<\eta$ can be represented also by the same treatment as follows:

$$\gamma^{\mathrm{BCS}}(\eta,t)\rightarrow\gamma^{\mathrm{BCS}}[\eta,\min(t,\xi)], \tag{15}$$

$$S(\eta,t)\rightarrow S[\eta,\min(t,\xi)]. \tag{16}$$

This approximation is very crude, however it is known to correctly describe the most divergent terms of each vertice. With this approximation together with the boundary conditions at the cutoff energy Λ for the Hubbard model,

$$\gamma_1(0,0)=U,\qquad \gamma_2(0,0)=0, \tag{17}$$

we can rearrange the parquet equations as follows.

(i) For $\eta<\xi$,

$$s_1(\eta,\xi)=U+N(0)\int_0^{\eta}dt\{[-2\sigma_1(t,\xi)+\sigma_2(t,\xi)]\gamma_1(t,\xi)+\sigma_1(t,\xi)\gamma_2(t,\xi)\}$$
$$+N(0)\int_{\eta}^{\xi}dt\{[-2\sigma_1(\eta,\xi)+\sigma_2(\eta,\xi)]\gamma_1(t,\xi)+\sigma_1(\eta,\xi)\gamma_2(t,\xi)\}, \tag{18}$$

$$s_2(\eta,\xi)=+N(0)\int_0^{\eta}dt\,\sigma_2(t,\xi)\gamma_2(t,\xi)+N(0)\int_{\eta}^{\xi}dt\,\sigma_2(\eta,\xi)\gamma_2(t,\xi). \tag{19}$$

(ii) For $\xi<\eta<\eta_0$,

$$\sigma_1(\eta,\xi)=U-N(0)\int_0^{\xi}dt\{s_1(\eta,t)\gamma_2(\eta,t)+s_2(\eta,t)\gamma_1(\eta,t)\}-N(0)\int_{\xi}^{\eta}dt\{s_1(\eta,\xi)\gamma_2(\eta,t)+s_2(\eta,\xi)\gamma_1(\eta,t)\}, \tag{20}$$

$$\sigma_2(\eta,\xi) = -N(0)\int_0^{\xi} dt\{s_1(\eta,t)\gamma_1(\eta,t) + s_2(\eta,t)\gamma_2(\eta,t)\} - N(0)\int_{\xi}^{\eta} dt\{s_1(\eta,\xi)\gamma_1(\eta,t) + s_2(\eta,\xi)\gamma_2(\eta,t)\}, \quad (21)$$

for $\eta_0 < \xi < \eta$ or $\eta_0 < \eta < \xi$, the divergence in the DW channel [Eqs. (18) and (19)] are cut off at η_0 by Fermi surface warping. The two solutions of parquet equations join smoothly at $\eta = \eta_0$. Following the treatment by Bychkov *et al.*,[5–7] we solve the parquet equations for ξ and $\eta < \eta_0$.

Substituting the variable separated form $\gamma_2(\eta,\xi) = A_2(\eta)B_2(\xi)$ the Eq. (19), we get

$$A_2(\eta) - N(0)\int_0^{\eta} \sigma_2(t,\xi)A_2(t)dt$$

$$-N(0)\int_{\eta}^{\xi} \sigma_2(\eta,\xi)A_2(t)dt = \frac{\sigma_2(\eta,\xi)}{B_2(\xi)}. \quad (22)$$

Differentiating each side of Eq. (22) by η and ξ, respectively, we get

$$N(0)A_2(\xi) = \frac{1}{B_2^2(\xi)}\frac{d}{d\xi}B_2(\xi), \quad (23)$$

$$\frac{\partial}{\partial\eta}\gamma_2(\eta) = \frac{\partial}{\partial\eta}\sigma_2(\eta,\xi). \quad (24)$$

Rearranging Eqs. (23) and (24),

$$\frac{d}{dt}\gamma_2(t,t) = \frac{\partial}{\partial\eta}\sigma_2(\eta,t)|_{\eta=t} + N(0)\gamma_2^2(t,t), \quad (25)$$

the other cases of $\eta < \eta_0$ can be treated in a similar way,

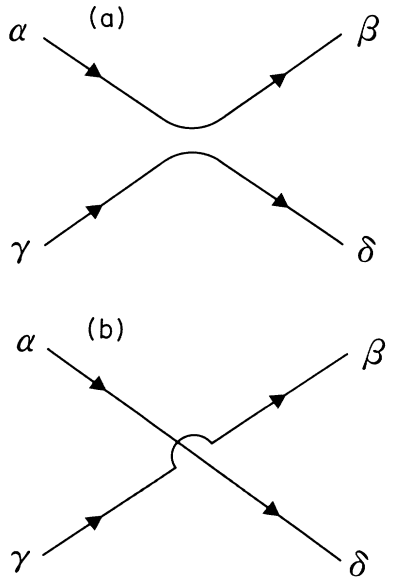

FIG. 4. (a) and (b) are backward and forward scatterings of which coupling constants are defined by $g_1(=\gamma_1)$ and $g_2(=\gamma_2-\gamma_1)$.

$$\frac{d}{dt}\gamma_3(t,t) = \frac{\partial}{\partial\eta}\sigma_3(\eta,t)|_{\eta=t} - 2N(0)\gamma_3^2(t,t), \quad (26)$$

$$\frac{d}{dt}\gamma_+(t,t) = \frac{\partial}{\partial\xi}s_+(t,\xi)|_{\xi=t} - N(0)\gamma_+^2(t,t), \quad (27)$$

$$\frac{d}{dt}\gamma_-(t,t) = \frac{\partial}{\partial\xi}s_-(t,\xi)|_{\xi=t} + N(0)\gamma_-^2(t,t), \quad (28)$$

where we have defined,

$$\begin{aligned}\gamma_+ &\equiv \gamma_1 + \gamma_2,\\ \gamma_- &\equiv \gamma_1 - \gamma_2,\\ \gamma_3 &\equiv \gamma_1 - \frac{1}{2}\gamma_2.\end{aligned} \quad (29)$$

For deriving Eqs. (26)–(28), we have used differential equations as follows.

For $\eta < \xi$ and $\eta < \eta_0$,

$$-2N(0)A_3(\xi) = \frac{1}{B_3^2(\xi)}\frac{d}{d\xi}B_3(\xi). \quad (30)$$

For $\xi < \eta < \eta_0$,

$$-N(0)B_+(\eta) = \frac{1}{A_+^2(\eta)}\frac{d}{d\eta}A_+(\eta), \quad (31)$$

$$N(0)B_-(\eta) = \frac{1}{A_-^2(\eta)}\frac{d}{d\eta}A_-(\eta). \quad (32)$$

In order to diagonalize the above equations, we rewrite Eqs. (25)–(28). Using from Eqs. (4)–(6), we arrange as follows:

$$\gamma_1 = \sigma_1 + s_1 - R_1 = \frac{1}{2}\sigma_2 + \sigma_3 + \frac{1}{2}s_1 + \frac{1}{2}s_2 - U, \quad (33)$$

$$\gamma_2 = \sigma_2 + s_2 - R_2 = \sigma_2 + \frac{1}{2}s_+ - \frac{1}{2}s_-. \quad (34)$$

Differentiating both sides of Eqs. (33) and (34) and using Eqs. (25)–(28), we get simplified sets of nonlinear equations:

$$\frac{d}{dt}\gamma_1(t,t) = -2N(0)\gamma_1^2(t,t), \quad (35)$$

$$\frac{d}{dt}\gamma_2(t,t) = -N(0)\gamma_1^2(t,t). \quad (36)$$

The solutions of Eqs. (35) and (36) with the boundary condition Eq. (17) are obtained in a straightforward way:

$$\gamma_1(t,t) = \frac{U}{1+2N(0)Ut}, \quad (37)$$

$$\gamma_2(t,t) = -\frac{1}{2}U + \frac{U}{2+4N(0)Ut}. \tag{38}$$

Using the variable separated forms, we can also calculate for $\xi < \eta < \eta_0$. For example, we solve γ_+. From definitions of the variable separate form, we get

$$\gamma_+(\eta,\xi) = \gamma_+(\xi,\xi)\frac{A_+(\eta)}{A_+(\xi)}. \tag{39}$$

From Eq. (23),

$$\frac{\frac{d}{d\eta}A_+(\eta)}{A_+(\eta)} = -N(0)\gamma_+(\eta). \tag{40}$$

Integrating Eq. (39), we get as follows:

$$A_+(\eta) = C\exp\left[-N(0)\int_0^\eta \gamma_+(t,t)dt\right], \tag{41}$$

where C is an integral constant.

Using Eqs. (37)–(41), we get a solution given by, for $\xi < \eta < \eta_0$,

$$\gamma_+(\eta,\xi) = \left[-\frac{1}{2}U + \frac{3}{2}\frac{U}{1+2N(0)U\xi}\right]\exp[\tfrac{1}{2}N(0)U(\eta-\xi)]\left[\frac{1+2N(0)U\xi}{1+2N(0)U\eta}\right]^{\frac{3}{4}}. \tag{42}$$

By the use of Eqs. (30)–(32), (37), and (38), the other solutions are given in a similar way.
For $\xi < \eta < \eta_0$,

$$\gamma_-(\eta,\xi) = \left[+\frac{1}{2}U + \frac{1}{2}\frac{U}{1+2N(0)U\xi}\right]\exp[\tfrac{1}{2}N(0)U(\eta-\xi)]\left[\frac{1+2N(0)U\eta}{1+2N(0)U\xi}\right]^{\frac{1}{4}}. \tag{43}$$

For $\eta < \xi < \eta_0$,

$$\gamma_2(\eta,\xi) = \left[-\frac{1}{2}U + \frac{1}{2}\frac{U}{1+2N(0)U\eta}\right]\exp[\tfrac{1}{2}N(0)U(\eta-\xi)]\left[\frac{1+2N(0)U\xi}{1+2N(0)U\eta}\right]^{\frac{1}{4}}, \tag{44}$$

$$\gamma_3(\eta,\xi) = \left[+\frac{1}{4}U + \frac{3}{4}\frac{U}{1+2N(0)U\eta}\right]\exp[\tfrac{1}{2}N(0)U(\eta-\xi)]\left[\frac{1+2N(0)U\eta}{1+2N(0)U\xi}\right]^{\frac{3}{4}}. \tag{45}$$

We find that the vertices for $\xi, \eta < \eta_0$ have a power favorable for density waves.

In the case of $\eta_0 < \xi$ and η, similarly, the results are obtained by the same method. The singularity of the DW channel is cut off by Fermi surface warping effects, because the parquet equations are given by the following.

(iii) For $\eta_0 < \eta < \xi$,

$$\begin{aligned} s_1(\eta,\xi) = \gamma_1(\eta_0,\eta_0) &+ N(0)\int_{\eta_0}^{\eta} dt\{[-2\sigma_1(t,\xi)+\sigma_2(t,\xi)]\gamma_1(t,\xi)+\sigma_1(t,\xi)\gamma_2(t,\xi)\} \\ &+N(0)\int_{\eta}^{\xi} dt\{[-2\sigma_1(\eta,\xi)+\sigma_2(\eta,\xi)]\gamma_1(t,\xi)+\sigma_1(\eta,\xi)\gamma_2(t,\xi)\}, \end{aligned} \tag{46}$$

$$s_2(\eta,\xi) = \gamma_2(\eta_0,\eta_0) + N(0)\int_{\eta_0}^{\eta} dt\,\sigma_2(t,\xi)\gamma_2(t,\xi) + N(0)\int_{\eta}^{\xi} dt\,\sigma_2(\eta,\xi)\gamma_2(t,\xi). \tag{47}$$

(iv) For $\eta_0 < \xi < \eta$,

$$\sigma_1(\eta,\xi) = \gamma_1(\eta_0,\eta_0), \tag{48}$$

$$\sigma_2(\eta,\xi) = \gamma_2(\eta_0,\eta_0). \tag{49}$$

The results for ξ and $\eta < \eta_0$ and for $\eta_0 < \xi$ and η are joined smoothly at η_0. The solutions of the parquet equations in this region are given as follows.

For $\eta_0 < \eta$ and ξ,

$$\gamma_2(\eta,\xi) = \frac{\gamma_2(\eta_0,\eta_0)}{1-N(0)(\xi-\eta_0)\gamma_2(\eta_0,\eta_0)}, \tag{50}$$

$$\gamma_3(\eta,\xi) = \frac{\gamma_3(\eta_0,\eta_0)}{1+2N(0)(\xi-\eta_0)\gamma_3(\eta_0,\eta_0)}, \tag{51}$$

where $\gamma_1(\eta_0,\eta_0)$ and $\gamma_2(\eta_0,\eta_0)$ are given by

$$\gamma_1(\eta_0,\eta_0) = \frac{U}{1+2UN(0)\eta_0}, \tag{52}$$

$$\gamma_2(\eta_0,\eta_0) = -\frac{U}{2} + \frac{U}{2+4UN(0)\eta_0}. \tag{53}$$

Superconducting and density-wave instabilities reveal themselves in the way the singularities of the vertices

appear for $\eta = \text{const}$, $\xi \to +\infty$ and $\eta \to \infty$, $\xi = \text{const}$, respectively. Equations (50) and (51) do not have singularities because the denominator is positive definite for $U > 0$. For finite doping, the singularity disappears by the warping effects of Fermi surfaces with the characteristic logarithmic energy scale η_0. At half filling, the vertex has a singularity only at $\eta = +\infty$.

We see from Eqs. (50) and (51) that the two-dimensional Hubbard model slightly doped near half filling does not have superconducting singularity even at zero temperature. The liquid state is a Fermi liquid in the strict sense that the momentum distribution function jumps finitely at the Fermi surface at zero temperature, and the excitations reach to MFL above the characteristic energy of Fermi surface warping.

III. THE EMERY MODEL

Now, let us study the Emery model[11–13] since it is more likely to have a superconducting instability. We restrict ourselves to the case in which the difference in atomic energy levels between oxygen $2p$ and copper $3d$ is much smaller than the hopping integrals of holes.[15,16] In this case, we can use the single-band Emery model given by

$$H_{\text{eff}} = \sum_{i,j\sigma}\left\{-t_R a^+_{i,\sigma}a_{j,\sigma} + \text{H.c.}\right\} + \sum_{i,\sigma}\frac{U_R}{2}\rho_{i,\sigma}\rho_{i,\sigma} + \sum_{i,j,\sigma,\sigma'} V_R\rho_{i,\sigma}\rho_{j,\sigma'}, \tag{54}$$

where the subscript R represents the renormalized value after the electrons on the copper site are integrated out, and i, j now runs over oxygen sites.

Here, we treat the Emery model by the same method used for the Hubbard model. The total vertex is represented by

$$\gamma_{\alpha\gamma\beta\delta} = \gamma_1(\delta_{\alpha\beta}\delta_{\delta\gamma} - \delta_{\alpha\delta}\delta_{\beta\gamma}) + \gamma_2\delta_{\alpha\delta}\delta_{\beta\gamma}. \tag{55}$$

The boundary conditions are given by

$$\gamma_1(0,0) = \frac{1}{2}U_R - V_{\text{eff}}, \tag{56}$$

$$V_{\text{eff}} \equiv V_R[\cos(k_{\text{F}x}a) + \cos(k_{\text{F}y}a)] \simeq 2V_R\cos\left(\frac{\pi}{2}\sqrt{1-\delta}\right), \tag{57}$$

where a is the lattice constant and δ is the ratio of hole doping.

For $\xi = \eta \equiv t < \eta_0$, the results are given by

$$\gamma_1(t,t) = \frac{U_R - 2V_{\text{eff}}}{2 + 2N(0)t[U_R - 2V_{\text{eff}}]}, \tag{58}$$

$$\gamma_2(t,t) = -\frac{1}{4}U_R + \frac{1}{2}V_{\text{eff}} + \frac{U_R - 2V_{\text{eff}}}{4 + 4N(0)t[U_R - 2V_{\text{eff}}]}. \tag{59}$$

(i) For $\xi < \eta < \eta_0$,

$$\gamma_+(\eta,\xi) = \left[-\frac{1}{4}(U_R - 2V_{\text{eff}}) + \frac{3}{4}\frac{U_R - 2V_{\text{eff}}}{1 + N(0)(U_R - 2V_{\text{eff}})\xi}\right] \times \exp[\tfrac{1}{4}N(0)(U_R - 2V_{\text{eff}})(\eta - \xi)]\left[\frac{1 + N(0)(U_R - 2V_{\text{eff}})\xi}{1 + N(0)(U_R - 2V_{\text{eff}})\eta}\right]^{\frac{3}{4}}, \tag{60}$$

$$\gamma_-(\eta,\xi) = \left[\frac{1}{4}(U_R - 2V_{\text{eff}}) + \frac{1}{4}\frac{U_R - 2V_{\text{eff}}}{1 + N(0)(U_R - 2V_{\text{eff}})\xi}\right] \times \exp[\tfrac{1}{4}N(0)(U_R - 2V_{\text{eff}})(\eta - \xi)]\left[\frac{1 + N(0)(U_R - 2V_{\text{eff}})\eta}{1 + N(0)(U_R - 2V_{\text{eff}})\xi}\right]^{\frac{1}{4}}. \tag{61}$$

(ii) For $\eta < \xi < \eta_0$,

$$\gamma_2(\eta,\xi) = \left[-\frac{1}{4}(U_R - 2V_{\text{eff}}) + \frac{1}{4}\frac{U_R - 2V_{\text{eff}}}{1 + N(0)(U_R - 2V_{\text{eff}})\eta}\right] \times \exp[\tfrac{1}{4}N(0)(U_R - 2V_{\text{eff}})(\eta - \xi)]\left[\frac{1 + N(0)(U_R - 2V_{\text{eff}})\xi}{1 + N(0)(U_R - 2V_{\text{eff}})\eta}\right]^{\frac{1}{4}}, \tag{62}$$

$$\gamma_3(\eta,\xi) = \left[+\frac{1}{8}(U_R - 2V_{\text{eff}}) + \frac{3}{8}\frac{U_R - 2V_{\text{eff}}}{1 + N(0)(U_R - 2V_{\text{eff}})\eta}\right] \times \exp[\tfrac{1}{4}N(0)(U_R - 2V_{\text{eff}})(\eta - \xi)]\left[\frac{1 + N(0)(U_R - 2V_{\text{eff}})\eta}{1 + N(0)(U_R - 2V_{\text{eff}})\xi}\right]^{\frac{3}{4}}. \tag{63}$$

For $\eta_0 < \eta, \xi$, the density-wave singularity is cut off by the warping effects. Using the same treatment as the Hubbard model, we write down the results given by

$$\gamma_2(\eta,\xi) = \frac{\gamma_2(\eta_0,\eta_0)}{1 - N(0)\gamma_2(\eta_0,\eta_0)(\xi - \eta_0)}, \tag{64}$$

$$\gamma_3(\eta,\xi) = \frac{\gamma_3(\eta_0,\eta_0)}{1 + 2N(0)\gamma_3(\eta_0,\eta_0)(\xi - \eta_0)}, \tag{65}$$

where $\gamma_1(\eta_0,\eta_0)$ and $\gamma_2(\eta_0,\eta_0)$ are given by

$$\gamma_1(\eta_0,\eta_0) = \frac{U_R - 2V_{\text{eff}}}{2 + 2(U_R - 2V_{\text{eff}})N(0)\eta_0}, \tag{66}$$

$$\gamma_2(\eta_0,\eta_0) = -\frac{U_R - 2V_{\text{eff}}}{4} + \frac{U_R - 2V_{\text{eff}}}{4 + 4(U_R - 2V_{\text{eff}})N(0)\eta_0}. \tag{67}$$

We find that, for $U_R - \frac{1}{2}V_{\text{eff}} > 0$, singularities of BCS and CDW type do not appear. For $U_R - \frac{1}{2}V_{\text{eff}} < 0$, CDW and spin-singlet s-wave-like superconductivity appear at the characteristic logarithmic energy scale as

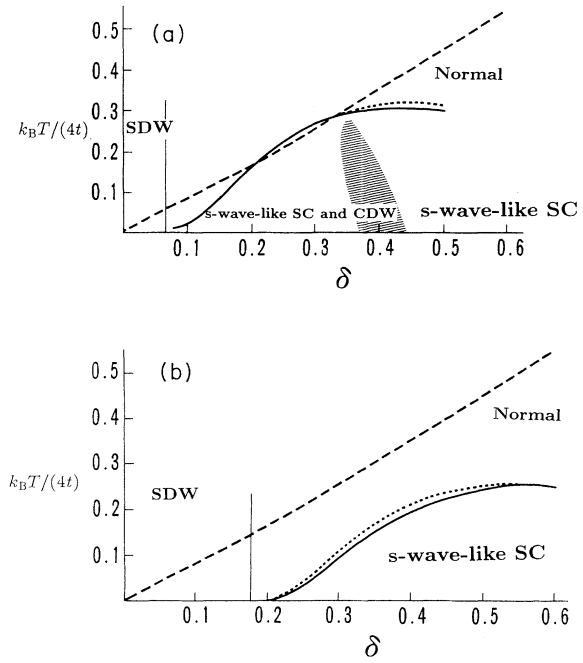

FIG. 5. Dependence of the characteristic energy scale of the CDW and singlet SC instability of the Emery model by hole doping. Dotted lines are a graph neglecting Fermi surface warping. Dashed lines describe the warping energy of Fermi surfaces. Crossover from CDW and spin-singlet s-wave-like superconductivity (SC) to spin-singlet s-wave-like SC is represented by a hatched region. We set (a) $V_R = 2$ eV and $U_R = 0.1$ eV, $1/N(0) = 2$ eV; and (b) $U_R = 1$ eV, $V_R = 1/N(0) = 2$ eV.

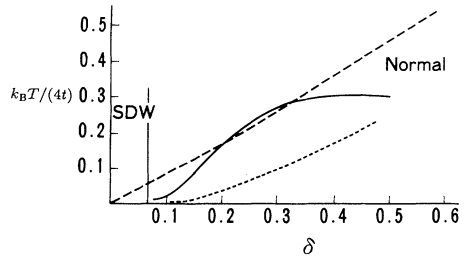

FIG. 6. Comparison between SC coupled to CDW with usual SC. The solid line is the characteristic energy of SC coupled to CDW. The dashed line shows the Fermi surface warping energy. The short-dashed line is the characteristic energy of usual BCS not coupled to CDW. We set $V_R = 1/N(0) = 2$ eV and $U_R = 0.1$ eV.

$$t_C = \frac{-1}{N(0)(U_R - 2V_{\text{eff}})}. \tag{68}$$

Let us now turn to the superconducting state which is stabilized for $U_R - 2V_{\text{eff}} < 0$. For $\eta_0 < \eta < \xi$, CDW divergence is suppressed by the Fermi surface warping, and only the spin-singlet s-wave-like superconductivity remains. The characteristic energy is $\Lambda \exp[-\eta_0 + \frac{1}{2N(0)\gamma_3(\eta_0,\eta_0)}]$. Of course, when the characteristic energy of CDW instability is larger than the characteristic energy of Fermi surface warping, CDW and singlet s-wave superconductivity appear at a temperature $\simeq \Lambda \exp[-t_C]$. We find that the warping effects reduce the characteristic energy of singlet s-wave superconductivity. This is shown in Figs. 5(a) and 5(b). We find that self-consistent coupling of polarization modes in comparison with usual superconductivity without coupling to CDW greatly enhances T_C as shown in Fig. 6, high T_C remains even by hole doping, as shown in Fig. 5.

The two-dimensional model is different from the one-dimensional superconductivity calculation[12,13] in that the umklapp g_3 scattering coupling constant can be ignored because of the Fermi surface warping. In one dimension, umklapp scattering cannot be ignored, and CDW is more enhanced. The Emery picture is thus recovered.

IV. THE EXTENDED HUBBARD MODEL WITH AN ISING-TYPE INTERACTION

In the previous section, we have investigated the effect of charge fluctuation for the Hubbard model. In this section, we shall study the effect of spin fluctuation. We restrict ourselves to the case in which the difference in atomic energy levels between oxygen $2p$ and copper $3d$ is much smaller than the hopping integrals of holes, so we can treat them by the single-band picture.[15,16] We start from an extended Hubbard model with an Ising-type interaction given by

$$H_{\text{eff}} = \sum_{i,j,\sigma} \left\{ -t_R a^+_{i,\sigma} a_{j,\sigma} + \text{H.c.} + 4J_R S^z_i S^z_j \right\} + \sum_{i,\sigma} \frac{U_R}{2} \rho_{i,\sigma} \rho_{i,\sigma}, \tag{69}$$

where the subscript R represents the renormalized value after the electrons on the copper site are integrated out.

Here, we treat the Hubbard with an Ising-type interaction by the same method used for the previous model. The total vertex is represented by

$$\gamma_{\beta\delta\alpha\gamma} = \gamma_1(\delta_{\alpha\beta}\delta_{\delta\gamma} - \delta_{\alpha\delta}\delta_{\beta\gamma}) + \gamma_2 \delta_{\alpha\delta}\delta_{\beta\gamma} + \gamma_z \sigma^z_{\alpha\delta}\sigma^z_{\beta\gamma}, \tag{70}$$

where σ^z is the z component of the Pauli matrix. In order to completely span the spin space, we have added $\gamma_z \sigma^z_{\alpha\delta}\sigma^z_{\beta\gamma}$.

The boundary conditions are given by

$$\gamma_1(0,0) = \frac{1}{2}U_R - \frac{1}{2}J_{\text{eff}}, \tag{71}$$

$$\gamma_2(0,0) = 0, \tag{72}$$

$$\gamma_z(0,0) = J_R[\cos(k_{\text{F}x}a) + \cos(k_{\text{F}y}a)] \simeq 2J_R \cos\left(\frac{\pi}{2}\sqrt{1-\delta}\right) \equiv J_{\text{eff}}, \tag{73}$$

where J_{eff} is a function of hole doping δ.

In order to separate the sets of parquet equations, we define a new set of vertices given by

$$\hat{\gamma}_1 \equiv -\gamma_1 + \gamma_2 - \gamma_z, \tag{74}$$

$$\hat{\gamma}_2 \equiv \gamma_2, \tag{75}$$

$$\hat{\gamma}_z \equiv \gamma_z. \tag{76}$$

Then, the boundary conditions are defined by

$$\hat{\gamma}_1(0,0) = -(\tfrac{1}{2}U_R + \tfrac{1}{2}J_{\text{eff}}) \equiv \hat{g}_1, \tag{77}$$

$$\hat{\gamma}_2(0,0) = 0 \equiv \hat{g}_2, \tag{78}$$

$$\hat{\gamma}_z(0,0) = J_{\text{eff}} \equiv \hat{g}_z. \tag{79}$$

Calculating by the same method as Secs. II and III, we write down the results for energy above the warping of Fermi surfaces as follows.

(a) For $\hat{g}_1 > 0$ and $\hat{g}_z > 0$, the results for $\xi = \eta = t$ are given by

$$\hat{\gamma}_1(t,t) = \frac{1}{2}(\hat{g}_1 + \hat{g}_z) + \sqrt{\hat{g}_1\hat{g}_z}A(t), \tag{80}$$

$$\hat{\gamma}_2(t,t) = \frac{1}{2}(\hat{g}_1 + \hat{g}_z) - \sqrt{\hat{g}_1\hat{g}_z}\sqrt{1 + A^2(t)}, \tag{81}$$

$$\hat{\gamma}_z(t,t) = \sqrt{\hat{g}_1\hat{g}_z}[-A(t) + \sqrt{1 + A^2(t)}], \tag{82}$$

where

$$A(t) \equiv \tan\left[\tan^{-1}\left(\frac{\hat{g}_1 - \hat{g}_z}{2\sqrt{\hat{g}_1\hat{g}_z}}\right) + 4N(0)\sqrt{\hat{g}_1\hat{g}_z}t\right], \tag{83}$$

when the argument of the tangent is $\pi/2$, the vertices have the singularity at a logarithmic energy scale as follows:

$$t_C \equiv \frac{1}{4N(0)\sqrt{\hat{g}_1\hat{g}_z}}\left[-\tan^{-1}\left(\frac{\hat{g}_1 - \hat{g}_z}{2\sqrt{\hat{g}_1\hat{g}_z}}\right) + \frac{\pi}{2}\right]. \tag{84}$$

We study the singular vertices of SC or DW type.

(i) For $\xi < \eta \to t_C$,

$$\hat{\gamma}_1 = 0, \tag{85}$$

$$\hat{\gamma}_0 = \infty, \tag{86}$$

$$\hat{\gamma}_{0+} = 0. \tag{87}$$

(ii) For $\eta < \xi \to t_C$,

$$\hat{\gamma}_{2+} = 0, \tag{88}$$

$$\hat{\gamma}_{2-} = 0, \tag{89}$$

$$\hat{\gamma}_3 = \infty, \tag{90}$$

where the vertices are defined by

$$\hat{\gamma}_{2+} = \hat{\gamma}_2 + \hat{\gamma}_z, \tag{91}$$

$$\hat{\gamma}_{2-} = \hat{\gamma}_2 - \hat{\gamma}_z, \tag{92}$$

$$\hat{\gamma}_3 = \hat{\gamma}_1 - \frac{1}{2}\hat{\gamma}_2 + \frac{1}{2}\hat{\gamma}_z, \tag{93}$$

$$\hat{\gamma}_{0+} = \frac{1}{2}\hat{\gamma}_1 + \hat{\gamma}_z. \tag{94}$$

The logarithmic energy scale t_C can be regarded as the characteristic logarithmic scale of phase transition. However, in the case of $t_C > \eta_0$, the SC singularity is suppressed and the SDW singularity is cut off at logarithmic scale η_0, because of the warping effect of the Fermi surfaces.

(b) For $\hat{g}_1 < 0$, $\hat{g}_z > 0$, $\xi = \eta = t \to +\infty$,

$$\hat{\gamma}_1 = -\sqrt{|\hat{g}_1\hat{g}_z|} + \frac{1}{2}(\hat{g}_1 + \hat{g}_z), \tag{95}$$

$$\hat{\gamma}_2 = \frac{1}{2}(\hat{g}_1 + \hat{g}_z), \tag{96}$$

$$\hat{\gamma}_z = +\sqrt{|\hat{g}_1\hat{g}_z|}. \tag{97}$$

(i) For $\xi < \eta \to +\infty$,

$$\hat{\gamma}_1(\eta,\xi) = \hat{\gamma}_1(\xi,\xi) \times\exp\left[-N(0)\left(\frac{\hat{g}_1+\hat{g}_z}{2} - \sqrt{\hat{g}_1\hat{g}_z}\right)(\eta-\xi)\right], \tag{98}$$

$$\hat{\gamma}_0(\eta,\xi) = \hat{\gamma}_0(\xi,\xi) \times\exp\left[-N(0)\left(\frac{\hat{g}_1+\hat{g}_z}{2} + \sqrt{\hat{g}_1\hat{g}_z}\right)(\eta-\xi)\right], \tag{99}$$

$$\hat{\gamma}_{0+}(\eta,\xi) = \hat{\gamma}_{0+}(\xi,\xi) \times\exp\left[-N(0)\left(\frac{\hat{g}_1+\hat{g}_z}{2} + \sqrt{\hat{g}_1\hat{g}_z}\right)(\eta-\xi)\right]. \tag{100}$$

(ii) For $\eta < \xi \to +\infty$,

$$\hat{\gamma}_{2+}(\eta,\xi) = \hat{\gamma}_{2+}(\eta,\eta) \times\exp\left[+N(0)\left(\frac{\hat{g}_1+\hat{g}_z}{2} + \sqrt{\hat{g}_1\hat{g}_z}\right)(\xi-\eta)\right], \tag{101}$$

$$\hat{\gamma}_{2-}(\eta,\xi) = \hat{\gamma}_{2-}(\eta,\eta) \times\exp\left[+N(0)\left(\frac{\hat{g}_1+\hat{g}_z}{2} - \sqrt{\hat{g}_1\hat{g}_z}\right)(\xi-\eta)\right], \tag{102}$$

$$\hat{\gamma}_3(\eta,\xi) = \hat{\gamma}_3(\eta,\eta) \times\exp\left[+N(0)\left(\frac{\hat{g}_1+\hat{g}_z}{2} - \sqrt{\hat{g}_1\hat{g}_z}\right)(\xi-\eta)\right]. \tag{103}$$

(c) For $\hat{g}_1 > 0$, $\hat{g}_z < 0$ and $\hat{g}_1 + \hat{g}_z > 0$, $\xi = \eta \to t'_C$,

$$\hat{\gamma}_1 = +\infty, \tag{104}$$

$$\hat{\gamma}_2 = -\infty, \tag{105}$$

$$\hat{\gamma}_z = \text{const.} \tag{106}$$

(i) For $\xi < \eta \to t'_C$,

$$\hat{\gamma}_1 = 0, \tag{107}$$

$$\hat{\gamma}_0 = +\infty, \tag{108}$$

$$\hat{\gamma}_{0+} = 0. \tag{109}$$

(ii) For $\eta < \xi \to t'_C$,

$$\hat{\gamma}_{2+} = 0, \tag{110}$$

$$\hat{\gamma}_{2-} = 0, \tag{111}$$

$$\hat{\gamma}_3 = +\infty, \tag{112}$$

where t'_C is given by

$$t'_C = \frac{1}{8N(0)\sqrt{\hat{g}_1\hat{g}_z}}\ln\left(\frac{\hat{g}_1-\hat{g}_z+2\sqrt{\hat{g}_1\hat{g}_z}}{\hat{g}_1-\hat{g}_z-2\sqrt{\hat{g}_1\hat{g}_z}}\right). \tag{113}$$

(d) For $\hat{g}_1 > 0$, $\hat{g}_z < 0$ and $\hat{g}_1 + \hat{g}_z < 0$, $\xi = \eta \to t'_C$,

$$\hat{\gamma}_1 = +\infty, \tag{114}$$

$$\hat{\gamma}_2 = +\infty, \tag{115}$$

$$\hat{\gamma}_z = -\infty. \tag{116}$$

(i) $\xi < \eta \to t'_C$,

$$\hat{\gamma}_1 = 0, \tag{117}$$

$$\hat{\gamma}_0 = 0, \tag{118}$$

$$\hat{\gamma}_{0+} = -\infty. \tag{119}$$

(ii) $\eta < \xi \to t'_C$,

$$\hat{\gamma}_{2+} = 0, \tag{120}$$

$$\hat{\gamma}_{2-} = +\infty, \tag{121}$$

$$\hat{\gamma}_3 = 0, \tag{122}$$

where t'_C is the same function as in (c).

(E) For $\hat{g}_1 < 0$ and $\hat{g}_z < 0$,

$$\hat{\gamma}_1(t,t) = \frac{1}{2}(\hat{g}_1+\hat{g}_z) + \sqrt{\hat{g}_1\hat{g}_z}A(t), \tag{123}$$

$$\hat{\gamma}_2(t,t) = \frac{1}{2}(\hat{g}_1+\hat{g}_z) + \sqrt{\hat{g}_1\hat{g}_z}\sqrt{1+A^2(t)}, \tag{124}$$

$$\hat{\gamma}_z(t,t) = \sqrt{\hat{g}_1\hat{g}_z}[-A(t) - \sqrt{1+A^2(t)}], \tag{125}$$

where

$$A(t) \equiv \tan\left[\tan^{-1}\left(\frac{\hat{g}_1-\hat{g}_z}{2\sqrt{\hat{g}_1\hat{g}_z}}\right) + 4N(0)\sqrt{\hat{g}_1\hat{g}_z}t\right]. \tag{126}$$

When the argument of the tangent in $A(t)$ is $\frac{\pi}{2}$, the vertices have the singularity at a logarithmic energy scale t_C which is the same form as in (a).

(e),(i) For $\xi < \eta \to t_C$,

$$\hat{\gamma}_1 = 0, \tag{127}$$

$$\hat{\gamma}_0 = 0, \tag{128}$$

$$\hat{\gamma}_{0+} = -\infty. \tag{129}$$

(e),(ii) For $\eta < \xi \to t_C$,

$$\hat{\gamma}_{2+} = 0, \tag{130}$$

$$\hat{\gamma}_{2-} = \infty, \tag{131}$$

$$\hat{\gamma}_3 = 0. \tag{132}$$

The tendency towards various instabilities for energy *higher* than $\Lambda \exp(-\eta_0)$ is summarized in the phase diagram in Fig. 7. In the $\hat{g}_1 < 0$ and $\hat{g}_z > 0$ case, the vertices have a singularity at zero energy, i.e., the state is a marginal phase between normal, SC, and SDW. The other cases have singularities at finite energy.

Now, in order to examine the ground state, we shall study Fermi surface warping effects for energies lower than $\Lambda \exp(-\eta_0)$. The vertices join smoothly at η_0 here again. The solution of the parquet equations for $\eta_0 < \eta$ and ξ is given by

$$\hat{\gamma}_{2+}(\eta, \xi) = \frac{\hat{\gamma}_{2+}(\eta_0, \eta_0)}{1 - N(0)\hat{\gamma}_{2+}(\eta_0, \eta_0)(\xi - \eta_0)}, \tag{133}$$

$$\hat{\gamma}_{2-}(\eta, \xi) = \frac{\hat{\gamma}_{2-}(\eta_0, \eta_0)}{1 - N(0)\hat{\gamma}_{2-}(\eta_0, \eta_0)(\xi - \eta_0)}, \tag{134}$$

$$\hat{\gamma}_3(\eta, \xi) = \frac{\hat{\gamma}_3(\eta_0, \eta_0)}{1 - 2N(0)\hat{\gamma}_3(\eta_0, \eta_0)(\xi - \eta_0)}. \tag{135}$$

Above the warping energy, the model with the AFM Ising interaction ($J_R > 0$) has a tendency to enhance SDW and singlet d-wave-like superconductivity with vertex singularity at zero energy; the parameters run to the upper left side as shown in Fig. 7. Below the warping energy, the superconducting state is barely able to appear. The phase diagram for AF Ising case is shown in Fig. 8. We see that the warping enhances superconductivity.

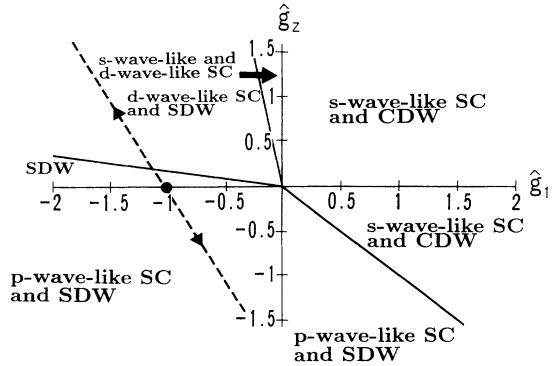

FIG. 7. Tendencies to instabilities of vertices between nested Fermi surfaces for the generalized Hubbard model with an Ising-type interaction *above* the low-energy cutoff ω_0. Phase boundaries are $\hat{g}_1 = \hat{g}_z = 0$, $\hat{g}_1 = -(3 + 2\sqrt{2})\hat{g}_z$, $\hat{g}_1 = -(3 - 2\sqrt{2})\hat{g}_z$, and $\hat{g}_1 = -\hat{g}_z$. We set $U_R = 4$ eV and $N^{-1}(0) = 2$ eV. With hole doping, the parameter runs along the dotted line. The small black circle shows the undoped case. Doping for $J_R > 0$ and $J_R < 0$, the parameters run toward the upper half-plane and lower half-plane, respectively.

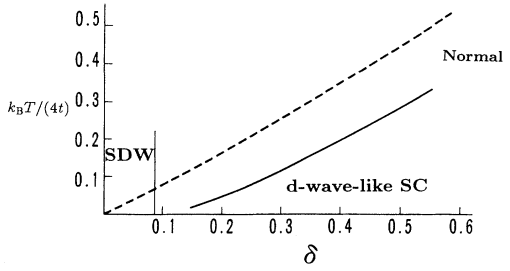

FIG. 8. Dependence of the characteristic energy scale of BCS instability by hole doping for $J_R > 0$. The dashed line corresponds to the warping energy of Fermi surfaces. We set the parameter as follows: $U_R/2 = 1/N(0) = 2$ eV and $J_R = 10$ eV.

In the FM case ($J_R < 0$), we see that the spin-density interaction term enhances the susceptibility of SDW and spin-triplet p-wave-like SC. The phase diagram for the FM Ising case is shown in Fig. 9. We see that the warping suppresses T_C contrary to the AFM Ising case.

V. DISCUSSION

Anomalous properties in the normal state of oxide superconductors are rather well described by NFL theory with a polarization mode of MFL type. We find that, at energies higher than $\Lambda \exp(-\eta_0)$, the extended models, such as the Emery model and the Hubbard model

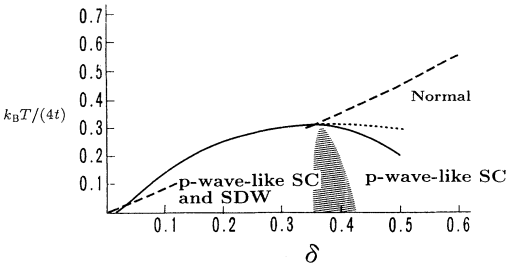

FIG. 9. Dependence of the characteristic energy scale of BCS instability by hole doping for $J_R < 0$. The dashed line corresponds to the warping energy of Fermi surfaces. The dotted line is a graph neglecting Fermi surface warping. The hatched region shows the crossover region from SDW and spin-triplet p-wave-like SC to spin-triplet p-wave-like SC. We set the parameters as follows: $U_R/2 = 1/N(0) = 2$ eV and $J_R = -1.4$ eV. A dashed line is the characteristic energy scale of Fermi surface warping.

with Ising interaction, have the same effect as the MFL-type polarization mode.[1,4] Below the energy $\Lambda \exp(-\eta_0)$, however, the models show Fermi-liquid behavior, essentially because the Fermi surface warping suppresses the density-wave instabilities.

Parquetlike coexistence of superconducting and density-wave instabilities gives important roles to the NFL polarization modes. The polarization mode enhances the attractive force and T_C. For $\eta_0 > t_C$, the density of state is enhanced above the logarithmic energy scale t_C and is suppressed rapidly below t_C. We find that the MFL-type polarization mode is in turn enhanced by SC and DW, so that the MFL-type polarization mode in the superconducting phase must be observed by a wide variety of experiments, including nuclear magnetic resonance and Raman scattering.[14] For $\eta_0 < t_C$, the MFL-type polarization mode is cut off by Fermi surface warping effects, and the vertex singularities are cut off by the maximum characteristic energy of SC, DW, and Fermi surface warping effects.

Now let us discuss our results in connection with the one-dimensional Emery model[7,12,13] examined with use of g-ology. In the calculation of Sec. III, we focused on hole doping in two dimensions. Therefore, g_3, the coupling constant for umklapp scattering, is unimportant due to the warping of Fermi surfaces. The two-dimensional Emery model has instabilities in CDW and singlet Cooper channels. Our results are consistent with the well-known g-ology results.[7,12] The only difference comes from the umklapp term, which is not important here.

VI. SUMMARY

We have studied superconductivity in NFL in two dimensions. Applying the parquet method of Bychkov *et al.*, we have treated self-consistently the coupling of superconductivity and density waves. We have taken into account the Fermi surface warping caused by hole doping by introducing the low-energy cutoff $\Lambda \exp(-\eta_0)$. This approximation is crude, but is sufficient for our parquet calculation in logarithmic accuracy.

We have examined the Hubbard model, Emery model, and a generalized Hubbard model with Ising-type exchange interactions. Although no superconductivity was found for the pure Hubbard model, we obtained superconducting phases for the latter two models. The calculated phase diagrams are found to be consistent with known theoretical results and experimental data for cuprate superconductors.

ACKNOWLEDGMENTS

We would like to thank Professor J. Ruvalds for sending his papers. We would like to thank Professor H. Fukuyama for communicating results prior to publication. We would like to thank Professor N. Nagaosa and our colleagues Dr. T. Ogawa and K. Semba for their valuable discussions. One of the authors (N.M.) would also like to thank Professor I. Ichinose and Dr. K-J. Hamada for valuable discussions. N.M. would also like to thank Dr. H. Yamamoto for various valuable ideas in the early stage of this study.

[1] C. M. Varma, P. B. Littlewood, S. Schmitt-Rink, E. Abrahames, and A. E. Rukenstein, Phys. Rev. Lett. **63**, 1996 (1989).

[2] G. T. Zimanyi and K. S. Bedell, Phys. Rev. Lett. **66**, 228 (1991).

[3] N. Mitani and S. Kurihara, in *Proceedings of the 2nd ISSP International Symposium on Physics and Chemistry of Oxide Superconductors, 1991* [Physica C **192**, 230 (1992)].

[4] A. Virosztek and J. Ruvalds, Phys. Rev. B **42**, 4064 (1990); Phys. Rev. Lett. **67**, 1657 (1991).

[5] Yu. A. Bychkov, L. P. Gor 'kov, and I. E. Dzyaloshinshii, Pis'ma Zh. Eksp. Teor. Fiz. **2**, 146 (1965) [JETP Lett. **2**, 92 (1965)]; Zh. Eksp. Teor. Fiz. **50**, 738 (1966) [Sov. Phys. JETP **23**, 489 (1966)].

[6] A. Bychkov's treatment (Ref. 5) is reviewed in detail by Nozieres *et al.*, see as follows, P. Nozieres, J. Gavoret, and B. Routlet, Phys. Rev. **178**, 1084 (1969).

[7] J. Solyom, Adv. Phys. **28**, 201 (1979).

[8] The model is investigated in detail by Schrieffer *et al.* We reconsider it from the viewpoint of the NFL theory. [J. R. Schrieffer, X. G. Wen, and S. C. Zhang, Phys. Rev. Lett. **60**, 944 (1988); Phys. Rev. B **39**, 11 663 (1989).]

[9] A. Kampf and J. R. Schrieffer, Phys. Rev. B **41**, 6399 (1990).

[10] In Sec. II, our result is consistent with a result of quantum Monte Carlo simulation by Hirsch [J. E. Hirsch, Phys. Rev. B **31**, 4403 (1985)].

[11] V. J. Emery, Phys. Rev. Lett. **58**, 2794 (1987).

[12] V. J. Emery, in *Highly Conducting One Dimensional Solids*, edited by J.T. De Vreese *et al.* (Plenum, New York, 1979).

[13] In one dimension, Emery investigated the Emery model (Ref. 11) in detail by treating Luttinger liquid which is a one-dimensional version of the NFL. He found that the pairing of soliton and antisoliton of the CDW phase mode is crucial for superconductors. [V. J. Emery, Phys. Rev. Lett. **65**, 1076 (1990).] In Sec. III, we investigated CDW instability in the Emery model in two dimensions from the viewpoint of NFL theory.

[14] For the coexistence of CDW and SC, this mode was investigated by Littlewood and Varma. [P. B. Littlewood and C. M. Varma, Phys. Rev. B **26**, 4883 (1982).] The amplitude mode of the SC interacts with the CDW phase mode with MFL-type polarization mode.

[15] In the strong atomic energy difference between oxygen and copper, Prelovsek investigated the model. He derived a simple two-band model where mobile charge carriers and spin excitations are predominantly oxygen $2p$ hole and localized $3d$ copper electrons, respectively, and oxygen holes and cop-

per electrons are Kondo coupled. [P. Prelovsek, Phys. Lett. **126**, 287 (1988); and Ref. 16.] On the other hand, the case of a small atomic energy difference between oxygen and copper can be treated only by a one-band picture.

[16] In the strong atomic energy difference between oxygen and copper, Kurihara *et al.* also investigated by means of a two-band picture from a viewpoint of phenomenology. [S. Kurihara, Phys. Rev. B **39**, 6600 (1989); N. Mitani and S. Kurihara, Physica C **206**, 13 (1993).]